Systems/Circuits

A High-Resolution *In Vivo* Atlas of the Human Brain's Serotonin System

Vincent Beliveau,[1,2] Melanie Ganz,[1] Ling Feng,[1] Brice Ozenne,[1,3] Liselotte Højgaard,[2,4] Patrick M. Fisher,[1] Claus Svarer,[1] Douglas N. Greve,[5,6] and Gitte M. Knudsen[1,2]

[1]Neurobiology Research Unit and Center for Integrated Molecular Brain Imaging, Rigshospitalet, [2]Faculty of Health and Medical Sciences, [3]Department of Public Health, Section of Biostatistics, and [4]PET and Cyclotron Unit, Copenhagen University Hospital, Rigshospitalet, DK-2100 Copenhagen, Denmark, [5]Athinoula A. Martinos Center for Biomedical Imaging, Department of Radiology, Massachusetts General Hospital, Boston, Massachusetts 02129, and [6]Harvard Medical School, Boston, Massachusetts 02115

The serotonin (5-hydroxytryptamine, 5-HT) system modulates many important brain functions and is critically involved in many neuropsychiatric disorders. Here, we present a high-resolution, multidimensional, *in vivo* atlas of four of the human brain's 5-HT receptors (5-HT_{1A}, 5-HT_{1B}, 5-HT_{2A}, and 5-HT_4) and the 5-HT transporter (5-HTT). The atlas is created from molecular and structural high-resolution neuroimaging data consisting of positron emission tomography (PET) and magnetic resonance imaging (MRI) scans acquired in a total of 210 healthy individuals. Comparison of the regional PET binding measures with postmortem human brain autoradiography outcomes showed a high correlation for the five 5-HT targets and this enabled us to transform the atlas to represent protein densities (in picomoles per milliliter). We also assessed the regional association between protein concentration and mRNA expression in the human brain by comparing the 5-HT density across the atlas with data from the Allen Human Brain atlas and identified receptor- and transporter-specific associations that show the regional relation between the two measures. Together, these data provide unparalleled insight into the serotonin system of the human brain.

Key words: 5-HT; atlas; autoradiography; MRI; mRNA; PET

Significance Statement

We present a high-resolution positron emission tomography (PET)- and magnetic resonance imaging-based human brain atlas of important serotonin receptors and the transporter. The regional PET-derived binding measures correlate strongly with the corresponding autoradiography protein levels. The strong correlation enables the transformation of the PET-derived human brain atlas into a protein density map of the serotonin (5-hydroxytryptamine, 5-HT) system. Next, we compared the regional receptor/transporter protein densities with mRNA levels and uncovered unique associations between protein expression and density at high detail. This new *in vivo* neuroimaging atlas of the 5-HT system not only provides insight in the human brain's regional protein synthesis, transport, and density, but also represents a valuable source of information for the neuroscience community as a comparative instrument to assess brain disorders.

Introduction

Serotonin (5-hydroxytryptamine, 5-HT) is a highly evolutionary conserved monoamine neurotransmitter that, across species, modulates multiple psychophysiological functions. In the human brain, 5-HT is synthesized within the brainstem's raphe nuclei, which have distributed efferent and afferent projections through-

Received Sept. 8, 2016; revised Nov. 8, 2016; accepted Nov. 12, 2016.

Author contributions: V.B., P.M.F., C.S., D.N.G., and G.M.K. designed research; V.B. and L.H. performed research; V.B., M.G., L.F., and B.O. analyzed data; V.B., M.G., L.F., B.O., L.H., P.M.F., C.S., D.N.G., and G.M.K. wrote the paper.

Collection of data included in the study was supported by the Lundbeck Foundation Center Cimbi (Grant R90-A7722). V.B. was supported by the Danish Council for Independent Research–Medical Sciences (Grant 4183-00627) and the Research Council of Rigshospitalet (R84-A3300). M.G. was supported by the Carlsberg Foundation (Grant 2013-01-0502) and the National Institutes of Health (Grant 5R21EB018964-02). L.F. was supported by the European Union's Seventh Framework Programme (Grant FP7/2007-2013 under Agreement HEALTH-F2-2011-278850 INMiND). D.N.G.'s research was supported by the National Institutes of Health (Multimodal Brain Imaging of Serotonin Grant 5R21EB018964-02) and the MGH Shared Instrumentation Grant S10RR023043). We thank the John and Birthe Meyer Foundation for providing the PET HRRT scanner.

G.M.K. has been an invited lecturer at Pfizer A/S, worked as a consultant and received grants from H. Lundbeck A/S, is a stock holder of Novo Nordisk/Novozymes, is on the board of directors of the BrainPrize and Elsass Foundation, is on the advisory board of the Kristian Jebsen Foundation, and has authored for Foreningen af Danske Lægestuderende and served as editor for Elsevier (International Journal of Neuropsychopharmacology). L.H. is chairman of the board of the Danish National Research Foundation, is on the board of the Science advisory board of the Olav Thon Foundation, and is chairman of the Advisory Board of European Union Horizon 2020, Health Demographic Change and Wellbeing. The remaining authors declare no competing financial interests.

Correspondence should be addressed to Gitte M. Knudsen, MD, DMSc, Neurobiology Research Unit, Rigshospitalet, 9 Blegdamsvej, Section 6931, DK-2100 Copenhagen, Denmark. E-mail: gmk@nru.dk.

DOI:10.1523/JNEUROSCI.2830-16.2016

Copyright © 2017 the authors 0270-6474/17/370120-09$15.00/0

Table 1. Demographics of healthy subjects

Receptor/transporter	5-HTT	5-HT_{1A}R	5-HT_{1B}R	5-HT_{2A}R	5-HT_4R
Radioligand	[^{11}C]DASB	[^{11}C]CUMI-101	[^{11}C]AZ10419369	[^{11}C]Cimbi-36	[^{11}C]SB207145
N	100	8	36	29	59
Gender (M/F)	29/71	3/5	24/12	15/14	41/18
Age (mean ± SD)	25.1 ± 5.8	28.4 ± 8.8	27.8 ± 6.9	22.6 ± 2.7	25.9 ± 5.3
BMI (kg/m^2, mean ± SD)	23.2 ± 2.9	22.7 ± 2.6	24.9 ± 4.3	23.4 ± 2.4	23.5 ± 3.3
Injected dose (MBq, mean ± SD)	586.0 ± 32.2	510.5 ± 149.1	585.4 ± 37.4	510.4 ± 109.7	577.1 ± 70.9
Injected mass (μg, mean ± SD)	1.9 ± 2.2	2.0 ± 1.5	1.2 ± 1.0	0.8 ± 0.5	1.1 ± 0.7

out the brain (Dorocic et al., 2014). The 5-HT system is highly diverse (Hannon and Hoyer, 2008). Based on structural, transductional, and operational features, its receptors have been grouped into seven families of receptors (5-HT_1 to 5-HT_7), including 14 known subtypes, and a transporter (5-HTT). Of the 14 receptors, there are 13 distinct G-protein-coupled receptors and one ligand-gated ion channel receptor, 5-HT_3. 5-HT is involved in myriad physiological functions such as cognition (Meneses, 1999), mood and social interaction (Young and Leyton, 2002), sexual behavior (Waldinger, 2015), feeding behavior (Magalhães et al., 2010), the sleep–wake cycle (Portas et al., 2000), and thermoregulation (Cryan et al., 2000). Disturbances in the 5-HT system are also linked to many debilitating brain disorders such as major depression, anxiety, and schizophrenia, as well as migraine and neurodegenerative disorders (Muller and Jacobs, 2009). The role of the individual receptors in the different functions and disorders is, however, only partially known. A prominent example is that, even though the 5-HTT inhibitors (selective serotonin reuptake inhibitors) are the most frequently prescribed antidepressant drug class, the exact involvement of individual 5-HT receptors in mediating their clinical effects is still unclear. To study the role of the individual receptors in healthy individuals, in patients with brain disorders, and in response to physiological or drug interventions, *in vivo* molecular brain imaging with positron emission tomography (PET) in conjunction with an appropriate radiotracer represents the state-of-the-art approach for quantifying the density and spatial distribution of brain receptors and transporters.

Brain atlases play a key role in neuroimaging research. Stereotactic atlases of magnetic resonance imaging (MRI) brain morphology such as the Talairach (Talairach and Tournoux, 1988) and the Montreal Neurological Institute (MNI) atlas (Evans et al., 1992) have become fundamental pillars for performing group analysis and anatomical segmentations such as the Automated Anatomical Labeling atlas (Tzourio-Mazoyer et al., 2002) are commonly used to report results of regional outcomes of brain imaging data. A high-resolution human brain atlas of 5-HT receptors will represent a valuable tool for neuroimaging studies investigating the 5-HT system and disorders related to its dysfunction.

The distribution of 5-HT receptors in the human postmortem brain has in the past been described extensively by autoradiography. However, autoradiography measurements, although quantitative, provide far less spatial information than a whole-brain atlas. With the development of well validated radioligands for imaging the 5-HT system *in vivo*, it is now possible to image specific 5-HT receptor subtypes and the 5-HTT. Up to now, specific and validated PET radioligands for use in humans have been developed for the receptors 5-HT_{1A}R, 5-HT_{1B}R, 5-HT_{2A}R, and 5-HT_4R and for 5-HTT (Paterson and Kornum, 2013). A radioligand for the 5-HT_6 receptor has been validated in humans (Parker et al., 2012), but was not included here because it also has high affinity to the 5-HT_{2A} receptor (Parker et al., 2015).

We here present an MRI- and PET-based high-resolution atlas of the human brain 5-HT receptors 5-HT_{1A}R, 5-HT_{1B}R, 5-HT_{2A}R, and 5-HT_4R and the 5-HTT, represented both in volume and on the cortical surface. The atlas was generated using a subset of the Center for Integrated Molecular and Brain Imaging's (Cimbi's) extensive database (Knudsen et al., 2015), including 210 healthy volunteers aged between 18 and 45 years. Regional PET binding values were compared with corresponding postmortem autoradiography data (Bonaventure et al., 2000; Varnäs et al., 2004), allowing us to validate our results and convert binding values into densities (Bmax). Furthermore, regional densities were compared with mRNA levels from the Allen Human Brain Atlas (Hawrylycz et al., 2012; French and Paus, 2015) to confirm previous findings and to gain novel insights into the localization of the receptor/transporter protein versus its expression.

Materials and Methods

Participants. All participants included in this study were healthy male and female controls from the Cimbi database (Knudsen et al., 2015); all data from this database are freely accessible. The data analysis was restricted to include individuals aged between 18 and 45 years. Participants were recruited by advertisement for different research protocols approved by the Ethics Committee of Copenhagen and Frederiksberg, Denmark. A total of 232 PET scans and corresponding structural MRI scans were acquired for 210 individual participants; 189 subjects had only one scan, 20 subjects had two scans, and a single had three scans. Demographics details are presented in Table 1.

PET and structural MRI. PET data were acquired in list mode on a Siemens HRRT scanner operating in 3D acquisition mode with an approximate in-plane resolution of 2 mm (1.4 mm in the center of the field of view and 2.4 mm in cortex; Olesen et al., 2009). PET frames were reconstructed using a 3D–OSEM–PSF algorithm (Comtat et al., 2008; Sureau et al., 2008). Scan time and frame length were designed according to the radiotracer characteristics. Dynamic PET frames were realigned using AIR 5.2.5 (Woods et al., 1992; see Table 2 for details on framing and realignment). T1- and T2-weighted structural MRI were acquired on four different Siemens scanners with standard parameters. All structural MRIs (T1 and T2) were unwarped offline using FreeSurfer's gradient_nonlin_unwarp version 0.8 or online on the scanner (Jovicich et al., 2006). For further details on structural MRI acquisition parameters, see Knudsen et al. (2015).

Further processing was performed with FreeSurfer 5.3 (Fischl, 2012; http://surfer.nmr.mgh.harvard.edu) using a surface and a volume stream. The individual cortical surfaces were reconstructed using the structural MRI corrected for gradient nonlinearities. The pial surfaces were further refined using T2-weighted structural images and corrected manually where necessary. PET–MR coregistration was estimated using boundary-based registration (Greve and Fischl, 2009) between the time-weighted sum of the PET time–activity curves (TACs) and the structural MRI. Additionally, the transformation from individual MR space to normal MNI152 space was estimated with combined volume–surface (CVS) registration (Postelnicu et al., 2009).

Regional TACs for the cortical regions were extracted by resampling the TACs to the cortical surface (Greve and Fischl, 2009) and taking the average within each of the 34 regions defined by the Desikan–Killiany

Table 2. PET scanning and realignment parameters

Radioligand	[^{11}C]DASB	[^{11}C]CUMI-101	[^{11}C]AZ10419369	[^{11}C]Cimbi-36	[^{11}C]SB207145
Scan time (min)	90	120	90	120	120
Frame lengths (number × sec)	6 × 10, 3 × 20, 6 × 30, 5 × 60, 5 × 120, 8 × 300, 3 × 600	6 × 5, 10 × 15, 4 × 30, 5 × 120, 5 × 300, 8 × 600	6 × 10, 6 × 20, 6 × 60, 8 × 120, 19 × 300	6 × 10, 6 × 20, 6 × 60, 8 × 120, 19 × 300	6 × 5, 10 × 15, 4 × 30, 5 × 120, 5 × 300, 8 × 600
Realigned frames (first:last)	10:36	10:38	13:45	13:45	10:38
Reference frame	26	26	27	27	26

cortical atlas (Desikan et al., 2006) automatically labeled by FreeSurfer. Similarly, regional TACs for seven subcortical regions were obtained by resampling the TACs to an MR-based refined version of the automatic volume segmentation derived by FreeSurfer for each subjects as described in Greve et al. (2016). In addition, a segmentation of cerebellum including different lobules (e.g., vermis) were created using SUIT 2.7 (Diedrichsen, 2006) and SPM12 (http://www.fil.ion.ucl.ac.uk/spm). Gray matter cerebellar segmentations used as reference region were created by limiting the FS segmentation to the intersection with the cerebellum labeled by SUIT, excluding vermis; this has the effect of removing peripheral overlabeling sometimes present in the cerebellar segmentations.

Due to the high binding of [^{11}C]DASB and [^{11}C]CUMI-101 within dorsal and median raphe, these ROIs can be delineated directly on PET images. Raphe TACs were obtained by delineating the ROIs on the time-weighted summed TACs using anatomical landmarks from structural MRI according to the method described in Beliveau et al. (2015) and extracting the average TACs within these regions. For the other tracers, raphe TACs were obtained by taking the average within normalized dorsal and median raphe templates. These templates were created by transferring the raphe ROIs previously derived to common space (MNI152) using CVS and taking the voxels with the highest overlap with a target volume of 150 mm^3 and 100 mm^3 for dorsal and median raphe, respectively. The delineations and templates were transferred back to PET space using CVS.

Subcortical voxelwise TACs in common volume space (MNI152) were obtained using CVS. Cortical vertexwise TACs in common surface space (fsaverage) were obtained using the cortical surface alignment estimated by FreeSurfer (Fischl et al., 1999). Finally, cortical and subcortical TACs were surface smoothed by 10 mm and volume smoothed by 5 mm full-width at half-maximum, respectively.

Kinetic modeling. For all radioligands, modeling of the parametric and regional nondisplaceable binding potential (BP_{ND}) was performed using the FS PET pipeline (Greve et al., 2013) with a Multilinear Reference Tissue Model 2 (MRTM2) (Ichise et al., 2003) using cerebellar gray matter, excluding vermis, as a reference region. The reference region washout rate (k_2') was computed using MRTM (Ichise et al., 1996); the high-binding TAC was obtained from a surface-weighted average of neocortical regions for [^{11}C]CUMI-101, [^{11}C]AZ10419369, and [^{11}C]Cimbi-36 and from a volume-weighted average of caudate and putamen for [^{11}C]SB207145 and of caudate, putamen, and thalamus for [^{11}C]DASB. Parametric and regional BP_{ND} were thresholded between 0 and 10 (outliers were set to the corresponding threshold value) and average maps were created. For 5-HTT, the TAC of the median raphe was found to be irreversible within the scan time, so the BP_{ND} for this region is not reported and it was disregarded from further analysis.

In vivo *binding and autoradiography.* To compare our results with those of Varnäs et al. (2004) and Bonaventure et al. (2000), regional values were adapted. First, the autoradiography data from Varnäs et al. (2004) was averaged across layers for individual cortical regions and divisions of subcortical structures were averaged to generate larger identifiable structures. Then, each region of the Desikan–Killiany cortical atlas (both left and right independently) and each subcortical region were grouped according to a set of regions common to the autoradiography data. Regional BP_{ND} values were then averaged within group using a volume/surface weighting. Regions where no reasonable pairing could be made were disregarded. The association between BP_{ND} and autoradiography was estimated using a linear regression without intercept because a null density is expected to yield null binding and the estimated slopes were used to transform BP_{ND} into density values. Pearson's and Spearman's correlation coefficients were also computed for all associations. The Shapiro–Wilks test was used to assess the normality of the residuals and the null hypothesis of normality was rejected for $p < 0.1$; whenever the residuals did not pass the test, only the Spearman's correlation coefficient is reported. Densities in units of picomoles per gram of tissue were converted to picomoles per milliliter using an approximate gray matter density of 1.045 g/ml (DiResta et al., 1991).

A linear mixed-effect model was used to investigate the global effect of age and gender on the regional density for the five 5-HT targets. The model included age, gender, and the interaction between age and gender as a fixed effect. Region-specific random effects were used to model regional-specific densities and subject-specific random effects to account for the correlation between the regional measurements of a given individual. To handle different variability in 5-HT density between regions, a separate variance parameter was estimated for each region. To investigate a possible regional-specific effect of age or gender, a separate linear regression was fitted to each region, including age, gender, and a possible interaction between age and gender as covariates. In the global models, the p-values were adjusted for multiple comparison over tracers ($n = 5$) controlling the false discovery at 5% (Benjamini and Hochberg, 1995). Similarly, regional models were corrected for multiple comparisons over regions ($n = 42$). For the entire analysis, the significance threshold was fixed at $p < 0.05$. Regional densities were averaged for left and right hemispheres.

The BP_{ND} of small volume of interest surrounded by low binding tissue can be drastically underestimated due to partial volume effects. As described previously (Savli et al., 2012), this is particularly pronounced in the raphe nuclei for the 5-HTT and 5-HT_{1A}R because there is high binding for the corresponding radioligand in this region, but much lower levels in to neighboring white matter tissue of the brainstem. Accordingly, the raphe nuclei density values reported here should be interpreted with caution and, although they are depicted in Figures 1 and 5, this region was excluded from any quantitative analysis for the 5-HTT and the 5-HT_{1A}R. Similarly, the 5-HTT BP_{ND} distribution within the globus pallidus was found to be highly heterogeneous due to partial volume effect from the caudate, so this region was also excluded from quantitative analysis for the 5-HTT.

In vivo *binding and mRNA levels.* Regional binding values were compared with 5-HT receptors and transporter mRNA normalized expression values from the Allen Human Brain Atlas (Hawrylycz et al., 2012). The atlas contains probe information from six human brains. Each probe is associated with mRNA levels (log2 intensity) for all genes sequenced, an anatomical label, and coordinates in the MNI152 space, as well as many other parameters. For more details on the materials and methods for the Allen Human Brain Atlas, see the Microarray Survey Technical White papers available at http://help.brain-map.org/display/humanbrain/Documentation. mRNA expression values for regions of the Desikan–Killiany cortical atlas were obtained from the work of French and Paus (2015). Each probe of the Allen Human Brain Atlas was paired to a cortical region using its coordinates in the MNI152 space and regional expression values were obtained by averaging expression values across probes, finding the median per region, and finally finding the median across subjects. We used the same approach to obtain subcortical expression values, but probes were paired to subcortical regions directly by their anatomical label rather than using their coordinates to identify corresponding regions. Both binding values and mRNA values were averaged between left and right hemispheres. As above, the association between binding and mRNA was estimated using a linear regression and

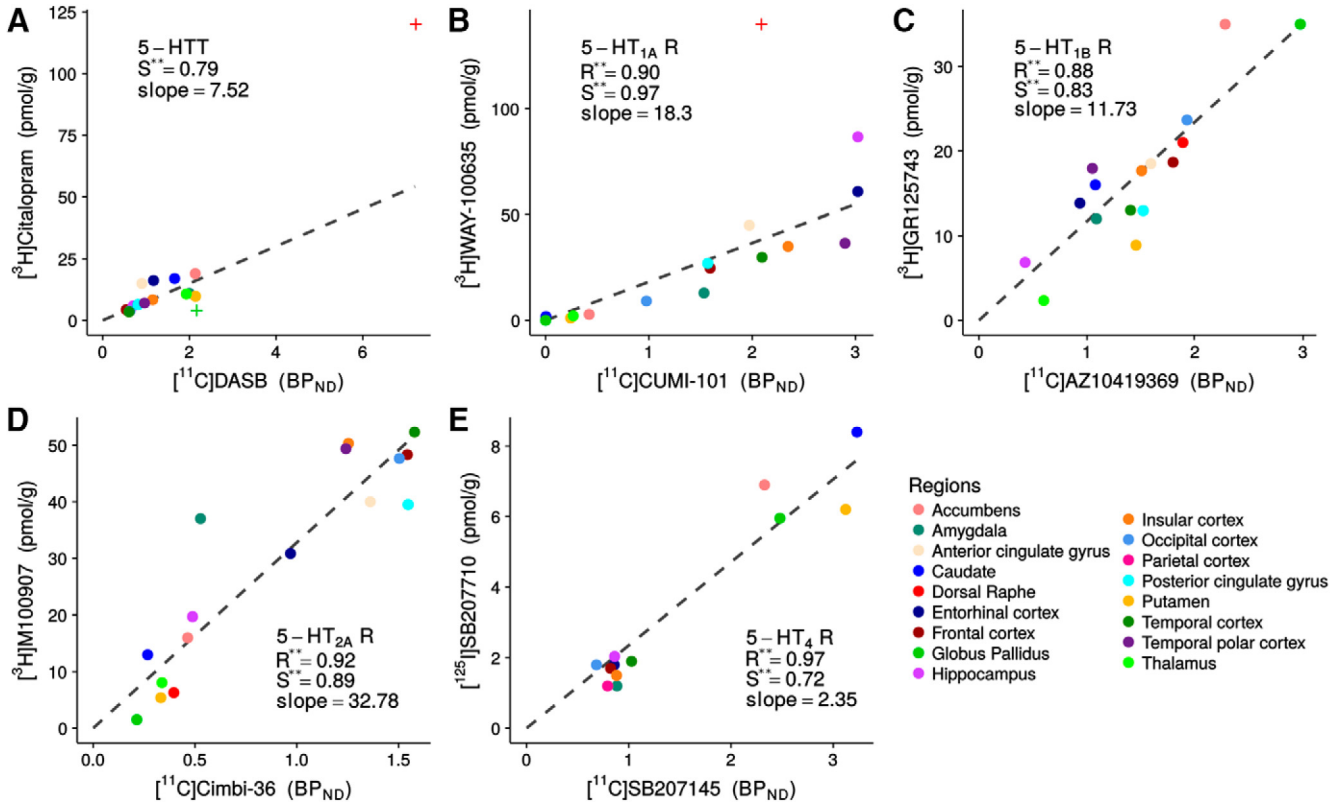

Figure 1. Regional BP_{ND} and B_{max} values for the five 5-HT targets: 5-HTT, 5-HT_{1A}R, 5-HT_{1B}R, 5-HT_{2A}R, and 5-HT_4R (***A–E***). The regions in the PET image space were combined to match the regions used by Varnäs et al. (2004) and Bonaventure et al. (2000) in their autoradiography measurement. The regressions (fixed through 0.0) are shown as black, dashed lines and the Pearson's (R) and Spearman's (S) correlation coefficients are reported. $^{**}p < 0.001$. Dorsal raphe, median raphe, and globus pallidus for 5-HTT and dorsal raphe for 5-HT_{1A}R were excluded from the regressions and marked with + on the figure (see Materials and Methods).

Pearson's and Spearman's correlation coefficients were also computed for all association. Dorsal raphe was excluded from the regression for 5-HTT and 5-HT_{1A}R and the regression was performed for cortical regions only for the 5-HT_{2A}R. For 5-HT_{1B}R and 5-HT_{2A}R, subcortical regions exhibited patterns distinct from the cortical regions, so the analysis was stratified between cortical and subcortical regions for these two targets.

Results

In vivo molecular imaging and autoradiography

Brain regional BP_{ND} values were compared with the corresponding receptor density measurements from postmortem autoradiography data from Varnäs et al. (2004) and Bonaventure et al. (2000) (for 5-HT_4R). Figure 1, *A–E*, shows the relation between autoradiography receptor/transporter B_{max} (density) from the two studies and PET measures of BP_{ND} from the Cimbi database. For all five targets, we found good to excellent associations between BP_{ND} and B_{max}, with Pearson's correlation coefficients ranging from 0.88 to 0.97 and Spearman's correlation coefficients ranging from 0.72 to 0.97. For 5-HTT, the residuals for 5-HTT did not pass the Shapiro–Wilks test for normality, so the Pearson's correlation is not reported for that association. The slope estimates of the regression were used to transform the BP_{ND} atlases into B_{max} atlases (Figs. 2,), allowing for a direct comparison across targets. The regional densities are presented in Figure 4. No global or regional significant effect of age, gender, or their interaction was found.

Receptor density and mRNA

The associations between *in vivo* receptor density, obtained by converting BP_{ND} into densities, and mRNA levels are shown in Figure 5. For the 5-HT_{1A}R, we found excellent correlation between the protein densities and mRNA levels, with Pearson's and Spearman's correlation coefficients of 0.94 and of 0.94, respectively. For 5-HT_4, the residuals did not pass the Shapiro–Wilks test for normality, but we found a moderate Spearman's correlation coefficient of 0.50. The 5-HT_{1B}R and 5-HT_{2A}R showed a distinctly different pattern compared with other targets, with good Pearson's correlation coefficients (0.66 and 0.60, respectively) and weak to moderate Spearman's correlation coefficients (0.28 and 0.46) in cortical regions, but there was no statistically significant correlation in subcortical regions.

Discussion

Here, we present the first high-resolution PET- and MRI-based *in vivo* human brain atlas of four 5-HT receptors and the transporter. The atlas highlights key features of the 5-HT targets, their spatial distribution, and abundance relative to each other. Because we identified high correlations with postmortem autoradiography receptor measurements, the atlas could be calibrated to represent absolute receptor or transporter densities, thus making it independent of the PET methodology in terms of choice of radiotracer and modeling approach. Access to such a high-resolution atlas of the 5-HT system enables scientists not only to evaluate the absolute densities of the individual targets, but also the relative abundance of protein and in any brain region of interest. However, a few caveats with this approach deserve to be mentioned here. Whereas autoradiography provides a measurement of the target density, PET returns an outcome measure that is proportional to the density of the target available for radioligand binding and the measure most notably depends on the *in*

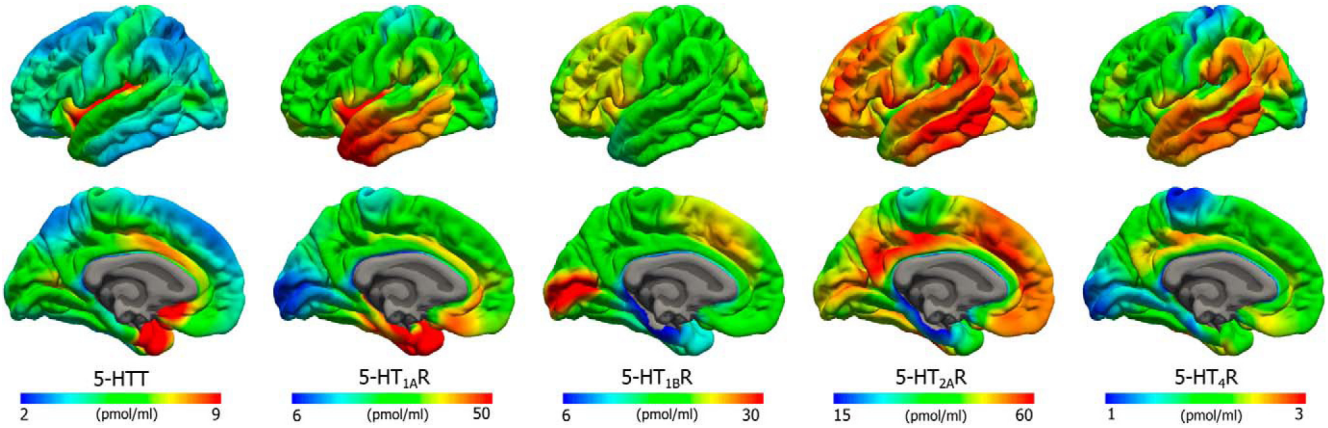

Figure 2. Average density (B_{max}) maps for five 5-HT targets on the common FreeSurfer surface (left hemisphere; lateral view, upper and medial view, lower). Color scaling was individually adjusted to highlight features of the distributions.

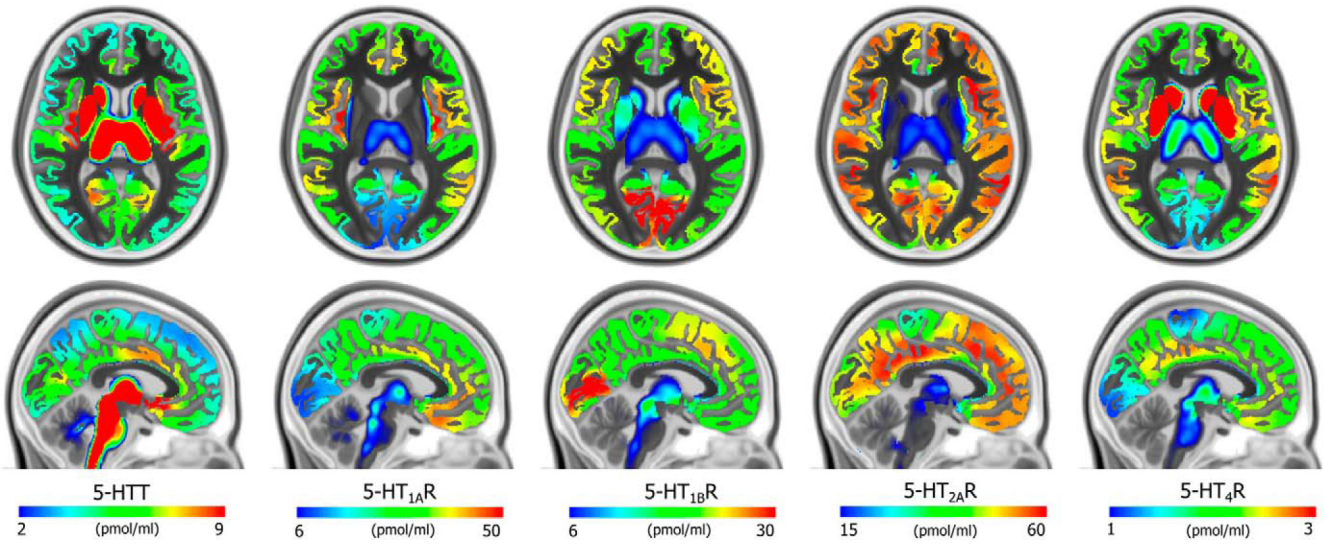

Figure 3. Average density (B_{max}) maps for the five 5-HT targets in the common MNI152 space (coronal, upper, $z = 8$ mm and sagittal, lower, $x = -3$ mm). Color scaling was individually adjusted to highlight features of the distributions.

vivo radioligand affinity to the target. However, because the occupancy of endogenous 5-HT is low for most targets (Paterson et al., 2010), it is unlikely that individual differences in endogenous 5-HT (and thereby *in vivo* affinity) would incur any bias.

Although PET imaging offers unique sensitivity and specificity, the intrinsic image resolution of PET is lower than for MRI. A prior brain 5-HT atlas has been reported based on PET scanners with a resolution of 4.4 mm and was generated independently of anatomical MRI (Savli et al., 2012). Leveraging high-resolution structural MRI (~1 mm resolution) in combination with molecular images acquired with a high-resolution PET scanner with a resolution of 2 mm allows for precise segmentation of brain regions and accurate intersubject normalization. The surface-based approach used in this work has also been shown to lead to a reduction in bias and variance of PET-derived measurements (Greve et al., 2013). A main advantage of the surface-based method is to diminish partial volume effects introduced by smoothing in the volume; smoothing on the surface drastically reduces the blurring of neighboring tissues with cortical gray matter and blurring across adjacent gyri (Hagler et al., 2006). Nevertheless, we still see subtle signs suggestive of partial volume effects; for example, bands of lower binding along the medial wall (Figure 6). Although a partial-volume-corrected atlas could be generated, we chose not to do so because methods for partial volume corrections come with their own set of limitations (Harri et al., 2007) and can lead to different results depending on the algorithm used (Greve et al., 2016).

Although [^{11}C]Cimbi-36 has been shown to have some affinity for 5-HT$_{2C}$, these receptors are mostly limited to the choroid plexus and the hippocampus. Furthermore, binding measures for [^{11}C]Cimbi-36 have been shown to be very strongly correlated to those of the 5-HT$_{2A}$ antagonist radiotracer [^{18}F]Altanserin (Ettrup et al., 2016). Therefore, any bias caused by the contribution of 5-HT$_{2C}$ receptors is expected to have minimal impact on the results presented here.

We compared our *in vivo* imaging atlases with meticulous autoradiography studies of the relevant 5-HT targets in postmortem human brain slices (Bonaventure et al., 2000; Varnäs et al., 2004). The postmortem brains in Varnäs et al. (2004) and Bonaventure et al. (2000) were retrieved from individuals older than those included in our study, with a respective mean age of 58 and 55 versus 26 years in our cohort. Therefore, the atlas densities represent those that can be observed in individuals matching the mean age of the population in the autoradiography studies.

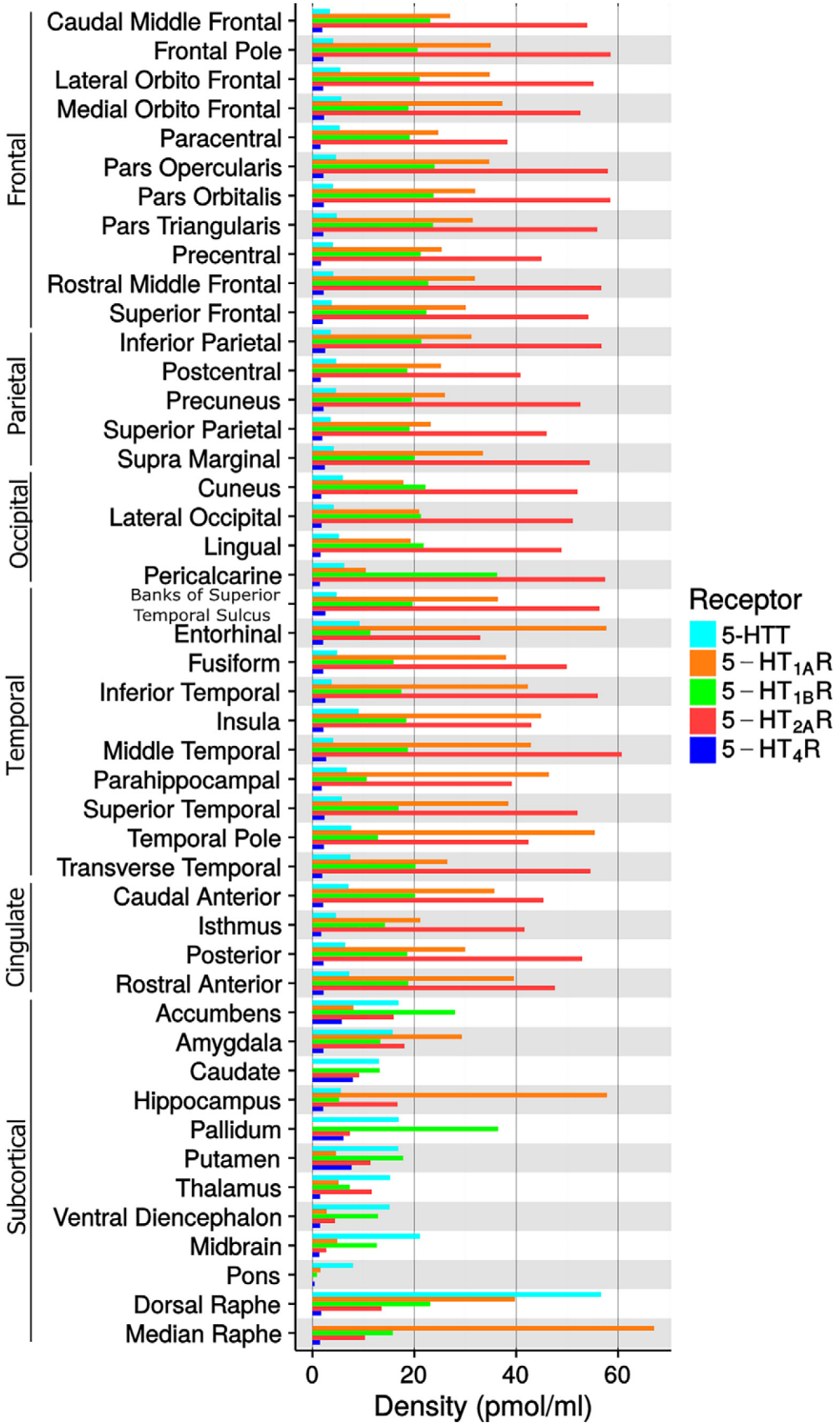

Figure 4. Density values (B_{max}) of the five 5-HT targets in FreeSurfer defined brain regions. Median raphe is not reported for 5-HTT due the irreversible kinetic of the TACs (see Material and Methods).

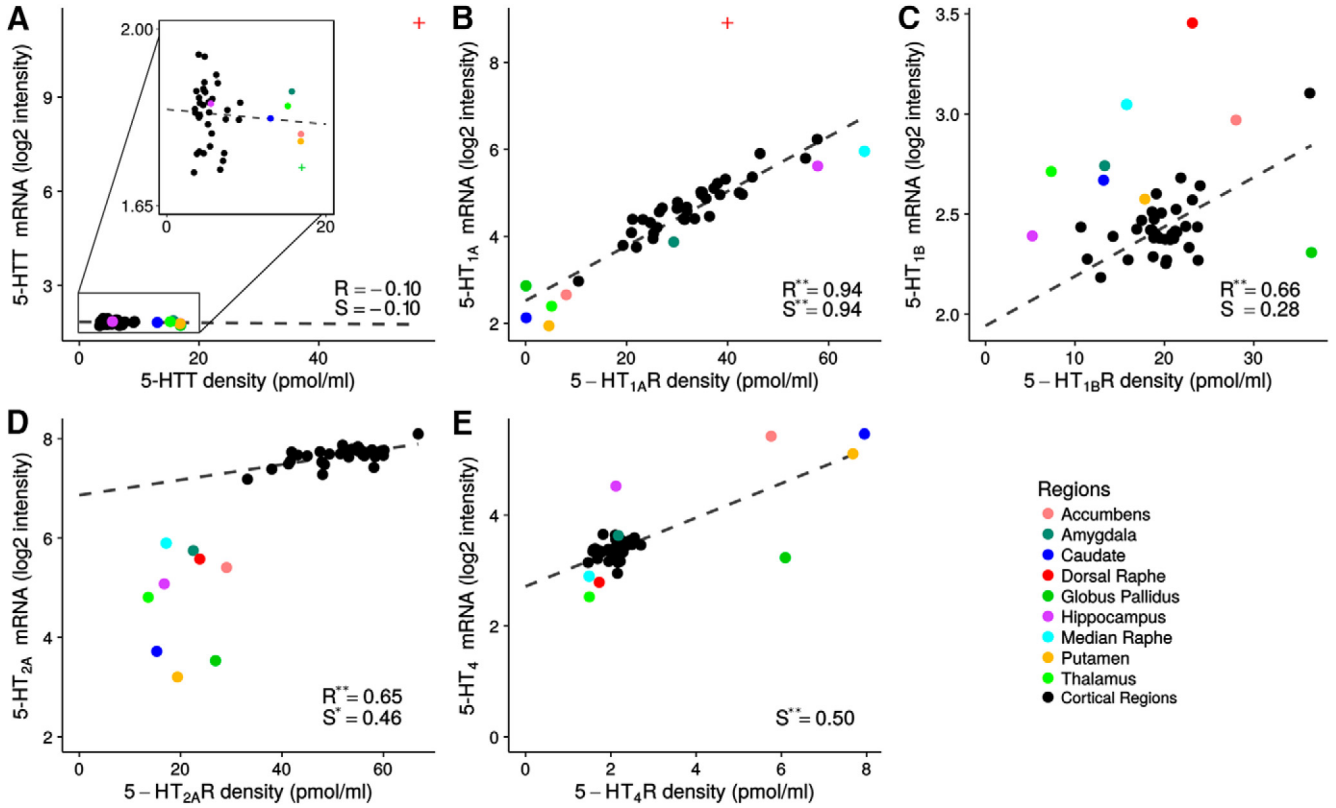

Figure 5. Regional density values (B_{max}) and mRNA levels for the five 5-HT targets: 5-HTT, 5-HT_{1A}R, 5-HT_{1B}R, 5-HT_{2A}R, and 5-HT_4R (***A–E***). Subcortical data are shown in color and cortical data are shown in black. The regression lines are shown as black dashed lines and the Pearson's (R) and Spearman's (S) correlation coefficients are reported. *$p < 0.01$; **$p < 0.001$. In ***C*** and ***D***, a line was fitted to cortical regions (black) only. Dorsal raphe, median raphe, and globus pallidus for 5-HTT and dorsal raphe for 5-HT_{1A}R were excluded from the regressions and marked with + on the figure (see Material and Methods).

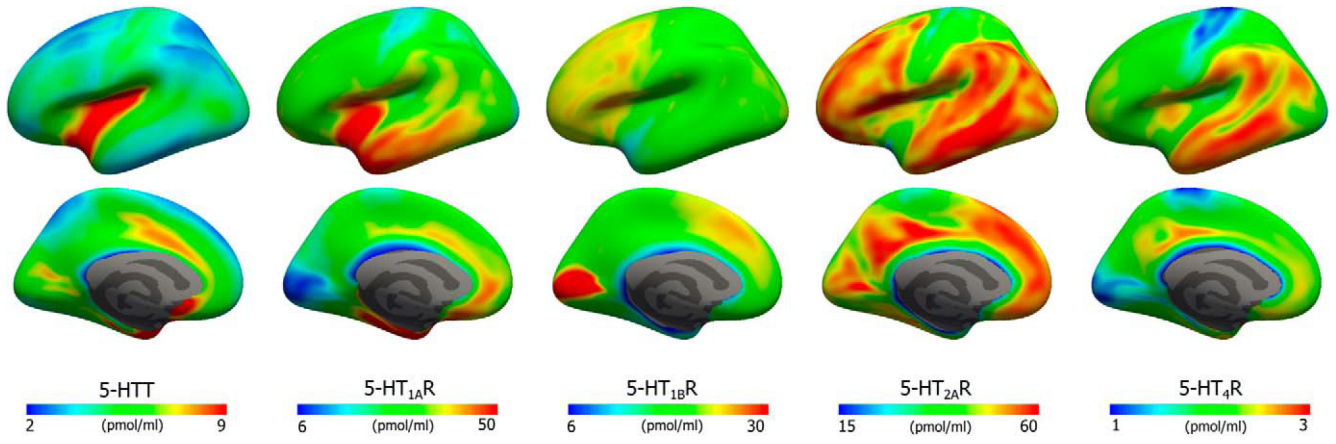

Figure 6. Average density (B_{max}) maps for five 5-HT targets on the inflated common FreeSurfer surface (left hemisphere; lateral view, upper and medial view, lower).

Within the current cohort, we did not observe any significant effect of age or gender within our data, most likely because of the limited age range of the subjects. Whereas some 5-HT targets, such as 5-HT_{1B}R and 5-HT_{2A}R, are relatively independent of age, others have been shown to have a pronounced age-dependent decline and/or sex differences (Moses-kolko et al., 2011; Nord et al., 2014). Therefore, minor data adjustments may be necessary when relating these atlases to specific research questions.

For all of the serotonergic targets, except for the 5-HT_{1A}R (Rizzo et al., 2014), we provide novel information about the relationship between *in vivo* molecular imaging in humans and the associated mRNA levels assessed in postmortem human brain tissue. The relation between the cerebral 5-HT target densities and their corresponding mRNA levels is of interest as mRNA levels often do not correspond to their protein levels because protein concentrations depend on the relative rates of transcription, mRNA decay, translation, and protein degradation (Vogel et al., 2010). Relating the two measures in brain space generates important information about the gene–protein translation. A high spatial correspondence between the two measures suggests that the protein is located on or at least close to the cell body, where the protein synthesis takes place. We found no significant association between 5-HTT mRNA and 5-HTT density, although, as expected, both were high in the dorsal raphe (Fig. 5*A*).

This is consistent with the exclusively presynaptic localization of 5-HTT and thus primary mRNA localization within raphe nuclei (Hoffman et al., 1998) and 5-HTT protein being located on terminal projections distant from 5-HT neurons (Zhou et al., 1998). The 5-HTT mRNA levels were overall low, both relative to the mRNA of other targets and to the 5-HTT protein density. Consistent with Rizzo et al. (2014), we found a very strong association between 5-HT_{1A}R mRNA and 5-HT_{1A}R protein density as determined with *in vivo* molecular neuroimaging (Fig. 5*B*). Rizzo et al. (2014) ascribed the tight correlation to a more general feature of the serotonergic system, but we show here that several other serotonergic targets show profound regional differences. We found a fair association between neocortical 5-HT_{1B}R mRNA and 5-HT_{1B}R density (Fig. 5*C*), but the subcortical regions did not conform to this association. As for the latter, our findings are consistent with a previous postmortem human brain study in which proportionally higher levels of 5-HT_{1B}R mRNA than protein were found, particularly in the ventral striatum, whereas the pallidum, the brain region with the highest 5-HT_{1B}R density, had low mRNA levels (Varnäs et al., 2005). This supports the observation in rodents that 5-HT_{1B}Rs in pallidum are localized in nerve terminals from striatal projections (Boschert et al., 1994) that are of GABAergic origin (Ghavami et al., 1999). To the best of our knowledge, existing literature does not provide evidence about the relative densities of 5-HT_{1B}R autoreceptors and heteroreceptors in different brain regions, but, due to the specific pattern observed here, we speculate that the 5-HT_{1B}R heteroreceptors may be relatively more abundant in subcortical regions. An interesting pattern of 5-HT_{2A}R mRNA versus 5-HT_{2A}R density emerged: whereas the neocortical brain regions showed a good, linear correlation, there was no association between the two measures in subcortical brain regions (Fig. 5*D*) and the neocortical and subcortical regions fall in two separate clusters on the graph. This pattern is in agreement with observations in the macaque monkey brain (López-Giménez et al., 2001) and suggests that the regulation and role of the 5-HT_{2A}R differ markedly between neocortical and subcortical brain regions, possibly because the 5-HT_{2A}R in neocortex are located in the apical part of pyramidal neurons (Jakab and Goldman-Rakic, 2000). In addition, the 5-HT_{2A}R mRNA levels are almost twice as high compared with the other investigated targets. We speculate that high mRNA levels enable the system to regulate synaptic 5-HT_{2A}R levels quickly, consistent with the ligand-induced endocytosis and recycling of 5-HT_{2A}R (Raote et al., 2013). We observed a moderate correlation association between 5-HT_4R mRNA and 5-HT_4R protein density (Fig. 5*E*). This finding is consistent with data obtained in humans, where 5-HT_4R mRNA levels and densities where high in caudate, putamen, accumbens, and the hippocampus formation and were both relatively lower in other brain regions.

Conclusion

Here, we present a comprehensive PET- and MRI-based high-resolution brain atlas of the serotonin system. By combining the *in vivo* atlases with postmortem autoradiography measurements, we calibrated the individual atlas to represent quantitative protein levels in terms of picomoles per milliliter. Furthermore, we describe the relation between regional serotonergic target densities and their mRNA levels, some for the first time in humans. The approach is generally applicable for any molecular target that can be visualized *in vivo* by PET. Such publicly available *in vivo* human brain atlases will serve as an important resource for neuroscience.

Notes

Supplemental material for this article is available at https://nru.dk/FS5ht-atlas. The surface and volume B_{max} maps presented in Figures 2 and 3 and a table containing regional B_{max} values from Figure 4 can be downloaded at this site. This material has not been peer reviewed.

References

Beliveau V, Svarer C, Frokjaer VG, Knudsen GM, Greve DN, Fisher PM (2015) Functional connectivity of the dorsal and median raphe nuclei at rest. Neuroimage 116:187–195. CrossRef

Benjamini Y, Hochberg Y (1995) Controlling the false discovery rate: a practical and powerful approach to multiple testing. J R Stat Soc Ser B 57:289–300.

Bonaventure P, Hall H, Gommeren W, Cras P, Langlois X, Jurzak M, Leysen JE (2000) Mapping of serotonin 5-HT(4) receptor mRNA and ligand binding sites in the post-mortem human brain. Synapse 36:35–46. CrossRef

Boschert U, Amara DA, Segu L, Hen R (1994) The mouse 5-hydroxytryptamine1B receptor is localized predominantly on axon terminals. Neuroscience 58:167–182. CrossRef

Comtat C, Sureau FC, Sibomana M, Hong IK, Sjoholm N, Trebossen R (2008) Image based resolution modeling for the HRRT OSEM reconstructions software. IEEE Nucl Sci Symp Conf Rec 2008:4120–4123.

Cryan JF, Harkin A, Naughton M, Kelly JP, Leonard BE (2000) Characterization of D-fenfluramine-induced hypothermia: evidence for multiple sites of action. Eur J Pharmacol 390:275–285. CrossRef

Desikan RS, Ségonne F, Fischl B, Quinn BT, Dickerson BC, Blacker D, Buckner RL, Dale AM, Maguire RP, Hyman BT, Albert MS, Killiany RJ (2006) An automated labeling system for subdividing the human cerebral cortex on MRI scans into gyral based regions of interest. Neuroimage 31:968–980. CrossRef

Diedrichsen JJ (2006) A spatially unbiased atlas template of the human cerebellum. Neuroimage 33:127–138. CrossRef

DiResta GR, Lee J, Arbit E (1991) Measurement of brain tissue specific gravity using pycnometry. J Neurosci Methods 39:245–251. CrossRef

Dorocic IP, Fürth D, Xuan Y, Johansson Y, Pozzi L, Silberberg G, Carlén M, Meletis K (2014) A whole-brain atlas of inputs to serotonergic neurons of the dorsal and median raphe nuclei. Neuron 83:663–678. CrossRef

Ettrup A, Svarer C, McMahon B, da Cunha-Bang S, Lehel S, Møller K, Dyssegaard A, Ganz M, Beliveau V, Jørgensen LM, Gillings N, Knudsen GM (2016) Serotonin 2A receptor agonist binding in the human brain with [(11)C]Cimbi-36: Test-retest reproducibility and head-to-head comparison with the antagonist [(18)F]altanserin. Neuroimage 34:1188–1196.

Evans AC, Collins DL, Milner B (1992) An MRI-based stereotactic atlas from 250 young normal subjects. Soc Neurosci Abstr 18:408.

Fischl B (2012) FreeSurfer. Neuroimage 62:774–781. CrossRef

Fischl B, Sereno MI, Tootell RBH, Dale AM (1999) High-resolution intersubject averaging and a coordinate system for the cortical surface. Hum Brain Mapp 8:272–284. CrossRef

French L, Paus T (2015) A FreeSurfer view of the cortical transcriptome generated from the Allen Human Brain Atlas. Front Neurosci 9:1–5.

Ghavami a, Stark KL, Jareb M, Ramboz S, Ségu L, Hen R (1999) Differential addressing of 5-HT1A and 5-HT1B receptors in epithelial cells and neurons. J Cell Sci 112 Pt 6:967–976.

Greve DN, Fischl B (2009) Accurate and robust brain image alignment using boundary-based registration. Neuroimage 48:63–72. CrossRef

Greve DN, Svarer C, Fisher PM, Feng L, Hansen AE, Baare W, Rosen B, Fischl B, Knudsen GM (2013) Cortical surface-based analysis reduces bias and variance in kinetic modeling of brain PET data. Neuroimage 92C:225–236.

Greve DN, Salat DH, Bowen SL, Izquierdo-Garcia D, Schultz AP, Catana C, Becker JA, Svarer C, Knudsen G, Sperling RA, Johnson KA (2016) Different partial volume correction methods lead to different conclusions: An 18F-FDG PET Study of aging. Neuroimage 132:334–343. CrossRef

Hagler DJ Jr, Saygin A, Sereno M, Hagler D (2006) Smoothing and cluster thresholding for cortical surface-based group analysis of fMRI data. Neuroimage 33:1093–1103. CrossRef

Hannon J, Hoyer D (2008) Molecular biology of 5-HT receptors. Behav Brain Res 195:198–213. CrossRef

Harri M, Mika T, Jussi H, Nevalainen OS, Jarmo H (2007) Evaluation of partial volume effect correction methods for brain positron emission to-

mography: quantification and reproducibility. J Med Phys 32:108–117. CrossRef
Hawrylycz MJ et al. (2012) An anatomically comprehensive atlas of the adult human brain transcriptome. Nature 489:391–399. CrossRef
Hoffman BJ, Hansson SR, Mezey E, Palkovits M (1998) Localization and dynamic regulation of biogenic amine transporters in the mammalian central nervous system. Front Neuroendocrinol 19:187–231. CrossRef
Ichise M, Ballinger J, Golan H (1996) Noninvasive quantification of dopamine D2 receptors with iodine-123-IBF SPECT. J Nucl Med 37:513–520.
Ichise M, Liow JS, Lu JQ, Takano A, Model K, Toyama H, Suhara T, Suzuki K, Innis RB, Carson RE (2003) Reference tissue parametric imaging methods: application to [11C] DASB positron emission tomography studies of the serotonin transporter in human brain. J Cereb Blood Flow Metab 23:1096–1112.
Jakab RL, Goldman-Rakic PS (2000) Segregation of serotonin 5-HT2A and 5-HT3 receptors in inhibitory circuits of the primate cerebral cortex. J Comp Neurol 417:337–348. CrossRef
Jovicich J, Czanner S, Greve D, Haley E, van der Kouwe A, Gollub R, Kennedy D, Schmitt F, Brown G, Macfall J, Fischl B, Dale A (2006) Reliability in multi-site structural MRI studies: effects of gradient non-linearity correction on phantom and human data. Neuroimage 30:436–443. CrossRef
Knudsen GM et al. (2015) The Center for Integrated Molecular Brain Imaging (Cimbi) Database. Neuroimage 124:1213–1219.
López-Giménez J, Vilaro TM, Palacios JM, Mengod G (2001) Mapping of 5-HT2A receptors and their mRNA in monkey brain: [3H]MDL100,907 autoradiography and in situ hybridization studies. J Comp Neurol 429: 571–589. CrossRef
Magalhães CP, de Freitas MFL, Nogueira MI, Campina RCDF, Takase LF, de Souza SL, de Castro RM (2010) Modulatory role of serotonin on feeding behavior. Nutr Neurosci 13:246–255. CrossRef
Meneses A (1999) 5-HT system and cognition. Neurosci Biobehav Rev 23: 1111–1125. CrossRef
Moses-kolko EL, Price JC, Shah N, Berga S, Sereika SM, Fisher PM, Coleman R, Becker C, Mason NS, Loucks T, Meltzer CC (2011) Age, sex, and reproductive hormone effects on brain serotonin-1A and serotonin-2A receptor binding in a healthy population. Neuropsychopharmacology 36: 2729–2740. CrossRef
Muller CP, Jacobs B (2009) Handbook of the Behavioral Neurobiology of Serotonin. Cambridge, MA: Academic Press.
Nord M, Cselenyi Z, Forsberg A, Rosenqvist G, Tiger M, Lundberg J, Varrone A, Farde L (2014) Distinct regional age effects on [11C]AZ10419369 binding to 5-HT1B receptors in the human brain. Neuroimage 103:303–308. CrossRef
Olesen OV, Sibomana M, Keller SH, Andersen F, Jensen J, Holm S, Svarer C, Højgaard L (2009) Spatial resolution of the HRRT PET scanner using 3D-OSEM PSF reconstruction. IEEE Nucl Sci Symp Conf Rec 2009:3789–3790.
Parker C a., Gunn RN, Rabiner E a., Slifstein M, Comley R, Salinas C, Johnson CN, Jakobsen S, Houle S, Laruelle M, Cunningham VJ, Martarello L (2012) Radiosynthesis and characterization of 11C-GSK215083 as a PET radioligand for the 5-HT6 receptor. J Nucl Med 53:295–303. CrossRef
Parker CA, Rabiner EA, Gunn R, Searle G, Martarello L, Comley R, Davy M, Wilson AA, Houle S, Mizrahi R, Laruelle M, Cunningham VJ (2015) Human kinetic modelling of the 5-HT6 PET radioligand, 11C-GSK215083, and its utility for determining occupancy at both 5HT6 and 5HT2A receptors by SB742457 as a potential therapeutic mechanism of action in Alzheimer's disease. J Nucl Med 56:1901–1909. CrossRef
Paterson L, Kornum B (2013) 5-HT radioligands for human brain imaging with PET and SPECT. Med Res Rev 33:54–111. CrossRef
Paterson LM, Tyacke RJ, Nutt DJ, Knudsen GM (2010) Measuring endogenous 5-HT release by emission tomography: promises and pitfalls. J Cereb Blood Flow Metab 30:1682–1706. CrossRef
Portas CM, Bjorvatn B, Ursin R (2000) Serotonin and the sleep/wake cycle: special emphasis on microdialysis studies. Prog Neurobiol 60:12–35.
Postelnicu G, Zollei L, Fischl B (2009) Combined volumetric and surface registration. Med Imaging IEEE Trans 28:508–522. CrossRef
Raote I, Bhattacharyya S, Panicker MM (2013) Functional selectivity in serotonin receptor 2A (5-HT2A) endocytosis, recycling, and phosphorylation. Mol Pharmacol 83:42–50. CrossRef
Rizzo G, Veronese M, Heckemann RA, Selvaraj S, Howes OD, Hammers A, Turkheimer FE, Bertoldo A (2014) The predictive power of brain mRNA mappings for in vivo protein density: a positron emission tomography correlation study. J Cereb Blood Flow Metab 34:827–835. CrossRef
Savli M, Bauer A, Mitterhauser M, Ding Y (2012) Normative database of the serotonergic system in healthy subjects using multi-tracer PET. Neuroimage 63:447–459. CrossRef
Sureau FC, Reader AJ, Comtat C, Leroy C, Ribeiro M-J, Buvat I, Trébossen R (2008) Impact of image-space resolution modeling for studies with the high-resolution research tomograph. J Nucl Med 49:1000–1008. CrossRef
Talairach J, Tournoux P (1988) Co-planar stereotaxic atlas of the human brain: 3-dimensional proportional system: an approach to cerebral imaging. Available online at https://www.researchgate.net/publication/283617540_Co-Planar_Stereotaxic_Atlas_of_the_Human_Brain3-Dimensional_Proportional_System_An_Approach_to_Cerebral_Imaging. Accessed November 28, 2016.
Tzourio-Mazoyer N, Landeau B, Papathanassiou D, Crivello F, Etard O, Delcroix N, Mazoyer B, Joliot M (2002) Automated anatomical labeling of activations in SPM using a macroscopic anatomical parcellation of the MNI MRI single-subject brain. Neuroimage 15:273–289. CrossRef
Varnäs K, Halldin C, Hall H (2004) Autoradiographic distribution of serotonin transporters and receptor subtypes in human brain. Hum Brain Mapp 22:246–260. CrossRef
Varnäs K, Hurd YL, Hall H (2005) Regional expression of 5-HT1B receptor mRNA in the human brain. Synapse 56:21–28. CrossRef
Vogel C, Abreu R de S, Ko D, Le S-YY, Shapiro BA, Burns SC, Sandhu D, Boutz DR, Marcotte EM, Penalva LO (2010) Sequence signatures and mRNA concentration can explain two-thirds of protein abundance variation in a human cell line TL-6. Mol Syst Biol 6:400.
Waldinger MD (2015) Psychiatric disorders and sexual dysfunction. Handb Clin Neurol 130:469–489. CrossRef Medline
Woods RP, Cherry SR, Mazziotta JC (1992) Rapid automated algorithm for aligning and reslicing PET images. J Comput Assist Tomogr 16:620–633. CrossRef
Young S, Leyton M (2002) The role of serotonin in human mood and social interaction: insight from altered tryptophan levels. Pharmacol Biochem Behav 71:857–865. CrossRef
Zhou FC, Tao-Cheng JH, Segu L, Patel T, Wang Y (1998) Serotonin transporters are located on the axons beyond the synaptic junctions: anatomical and functional evidence. Brain Res 805:241–254. CrossRef